Pre- and post-oxidation Raman analysis of $(U,Ce)O_2$ oxides

J. M. Elorrieta[1*], L. J. Bonales[1], S. Fernández[1], N. Rodríguez-Villagra[1], L. Gutiérrez-Nebot[1], V. G. Baonza[2] and J. Cobos[1]

[1] Centro de Investigaciones Energéticas, Medioambientales y Tecnológicas, CIEMAT, Avenida Complutense 40, 28040 Madrid, Spain

[2] MALTA-Consolider Team, Dep. Química Física, Fac. Ciencias Químicas, Universidad Complutense and Instituto de Geociencias IGEO (CSIC-UCM), 28040 Madrid, Spain

* CORRESPONDING AUTHOR

jmelorrieta@gmail.com

Centro de Investigaciones Energéticas, Medioambientales y Tecnológicas, CIEMAT.

Departamento de Energía. Unidad de Residuos de Alta Actividad.

Av. Complutense, 40, 28040 Madrid, Spain

Telephone number: + 34 913460841

ABSTRACT

A pre- and post-oxidation detailed Raman analysis has been carried out on a variety of $(U_{1-y},Ce_y)O_{2-x}$ oxides (y = 0.01, 0.03, 0.10, 0.15, 0.40). The changes undergone in the Raman spectrum of UO_2 as a function of Ce incorporation have been examined, thus extracting valuable information on the structural features and changes of these solid solutions, including the presence of vacancies in the cations' surroundings. Comparison of the results extracted from the post-oxidation analyses of Ce-containing samples with those obtained for pure UO_2 confirms that a Ce content as low as 1 mol% leads to a protective effect on the dioxide matrix against oxidation and that, under identical conditions, the oxidation process is slowed down as Ce concentration increases.

KEYWORDS

Uranium-cerium oxides, Raman spectroscopy, Oxidation.

1. INTRODUCTION

Uranium-cerium mixed oxides deserve special attention when addressing the stability of uranium-based spent nuclear fuel. This is not only because Ce is one of the fission products that is present in greater proportion in this type of fuel,[1] but also because of the frequent use of CeO_2 to simulate highly radioactive PuO_2 in the MOX fuel.[2-4]

CeO_2 and UO_2 have similar structural properties, presenting both fluorite-type cubic ordering, which promotes the formation of solid solutions when combined.[2,5] In such (U, Ce)O_2 mixed oxides, charge transfer between U^{4+} and Ce^{4+} ions has been widely reported.[1,6-9] While uranium tends to oxidise (up to U^{5+} and U^{6+}), cerium tends to reduce to its lower oxidation state (Ce^{3+}). The proportion of each chemical state of U and Ce in a given (U, Ce)O_2 oxide is strongly dependent on Ce content, as observed by Bera *et al.* in their detailed XPS analysis.[1] These authors suggested that reduction from Ce^{4+} to Ce^{3+} results in the creation of defects, specifically in the form of stable oxygen vacancies.

To understand the oxidation behaviour of (U, Ce)O_2 and to explain how the chemical states of U and Ce evolve during this reaction, a couple of studies have been carried out at high temperatures (> 500ºC), mainly focused on X-ray diffraction data.[2,4] In these studies, an oxidation hindering effect has been observed as Ce content increases. For instance, in both cases,[2,4] for $y < 0.4$ –in $(U_{1-y}Ce_y)O_{2\pm x}$– oxidation of the solid solutions leads to a mixture of an orthorhombic M_3O_8 phase (M=U,Ce) and a cubic M_4O_9 or MO_{2+x} phase, while for $y > 0.4$ M_3O_8 is no longer observed. In addition, Kumar *et al.*[4] detected the sole presence of Ce^{4+} ions in the oxidised samples, what might indicate that the initially existing oxygen vacancies disappear before uranium oxidation begins.

Despite the valuable information that could be extracted from Raman spectroscopy, especially with regard to the monitoring of oxygen vacancies observed on other mixed oxides,[10-14] there is only one study that applies this technique to acquire a better understanding of uranium-cerium dioxides.[15] Furthermore, there is no account of Raman analyses on their oxidation products. Therefore, this

paper presents for the first time a thorough Raman characterisation of a variety of (U, Ce)O_2 oxides, paying special attention to the evolution of the UO_2 Raman spectrum as Ce content increases, with the aim of understanding the changes occurring due to the incorporation of Ce. In addition, a post-oxidation Raman analysis is also addressed, in particular by comparing the spectra corresponding to the different oxidised samples to show the sensitivity of this technique to detect the influence of Ce concentration on the oxidation of mixed dioxides.

2. EXPERIMENTAL

Sample preparation

The starting UO_2 and CeO_2 powders, both with an average particle size of ~15 μm, were provided by ENUSA and Alfa Aesar, respectively. These materials were mixed in the intended proportions, together with 3% w/w of EBS (Ethyl Bis Stearamide, supplied by Tokyo Chemical Industry Co.) as binder and lubricant,[16] using low-energy ball milling. Following a conventional metallurgical procedure, the mixtures obtained were subjected to uniaxial pressing at 700 MPa. Subsequently, a heating process under a N_2-4.7%H_2 flow –in order to avoid UO_2 oxidation– was conducted on all the pre-sintered pellets, applying four consecutive steps: three isotherms at 100ºC (2h), 300ºC (4h) and 500ºC (4h) for calcination of the incorporated EBS, followed by the sintering isotherm at 1600ºC for 4 hours. The binder proportion used, applied pressure and sintering cycle were established elsewhere[17] and adapted to this study. Polishing and thermal annealing were then carried out, which consisted in a 10 minutes treatment at 1520ºC (95% of the sintering temperature) under the same N_2-4.7%H_2 atmosphere. As a result, a series of $(U_{1-y}Ce_y)O_{2-x}$ homogeneous solid solutions, with y = 0.01, 0.03, 0.10, 0.15 and 0.40, were obtained. It should be noted that the formula (U, Ce)O_{2-x} will be hereafter used with the aim of pointing out the presence of oxygen vacancies detected in these mixed oxides. The undoped UO_2 disk used as a reference was also supplied by ENUSA, while pure CeO_2 characterised for extrapolation was previously fabricated following the procedure reported in Ref. 17.

Oxidation procedure

The oxidation of the UO_2 and (U, Ce)O_{2-x} samples was performed by a Linkam THMS600 temperature controlled stage. The mechanical design and electronics of the Linkam stage provided precise control and stability of the temperature better than 0.2 degrees. A 10°C/min heating ramp was applied to reach the isothermal temperature, 350ºC, which was then maintained for 3 hours. A

dry air flow was supplied throughout the process. Cooling was subsequently conducted with the help of the in-house refrigeration system.

Characterisation techniques

X-ray diffraction measurements on the mixed oxides were carried out by a Bruker D8 Advance Eco diffractometer, using Cu Kα radiation (λ = 1.54056 Å) and operating at 40 kV and 25 mA. The Bragg-Brentano configuration geometry was used.

Raman spectroscopy analyses were performed with a Horiba LabRAM HR Evolution spectrometer. All spectra were acquired at an excitation wavelength of 632.8 nm provided by a He-Ne laser. The scattered radiation was then collected in backscattering geometry, dispersed using a 600 grooves/mm holographic grating and recorded using a CCD detector (256 x 1024 pixels), obtaining a ~1 cm^{-1}/pixel spatial resolution and a spectral resolution of better than 3 cm^{-1}. The obtained spectra were calibrated with the emission lines of a Ne lamp. The scattered radiation was collected through a 100x objective for characterisation of the pre-oxidation samples, while a 50x long focal distance objective was used to probe the oxidised samples in order to average the signal and to minimise the effect of the surface irregularities formed during oxidation. In all cases, the excitation power was minimised to avoid alteration of the samples.

3. RESULTS AND DISCUSSION

Pre-oxidation characterisation

Prior to oxidation, a systematic X-ray diffraction and Raman characterisation of all samples was performed. Figure 1 shows the values of the lattice parameters measured for the undoped UO_2 disk and the sintered $(U_{1-y}Ce_y)O_{2-x}$ oxides ($0.01 \leq y \leq 0.40$), assuming that the cubic structure of UO_2 prevails. The estimated lattice parameter value for pure CeO_2, which is consistent with literature values,[18] has also been included.

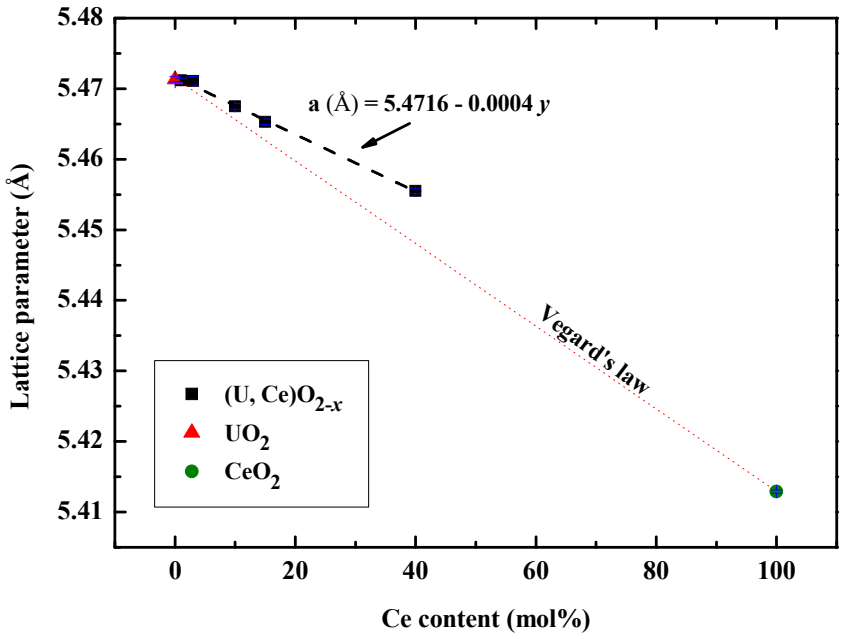

Fig. 1. Lattice parameter values estimated for pure UO_2 and the sintered $(U_{1-y}Ce_y)O_{2-x}$ oxides, with $0.01 \leq y \leq 0.40$. The lattice parameter value obtained for pure CeO_2 is also included.

A steady contraction of the lattice parameter is observed as Ce content increases (dashed line and equation inserted in Figure 1), as is expected from the partial substitution of U^{4+} ions by the smaller Ce^{4+} ions.[19] However, these data do not follow Vegard's law, as they do not fall on a straight line between the pure UO_2 and CeO_2 values (dotted line in Figure 1). Some of the earlier studies on (U, Ce)O_2 oxides were in good agreement with Vegard's law[19,20] and attributed such behaviour to a near-stoichiometric state of their oxides.[20] In our case, an increasing deviation towards higher lattice

parameter values, with regard to those predicted by Vegard's law, is observed as a function of Ce content. This would therefore imply that formation of stable oxygen vacancies had occurred in our samples, most likely related to an increasing presence of Ce^{3+} ions[1] (presenting larger atomic radii than Ce^{4+} ions[21]), leading to an expansion of the lattice (*e.g.* ~0.4 % for 40 mol% of Ce).[22]

Results of Raman characterisation are shown in Figure 2. Each spectrum actually consists of the average of 10 spectra acquired on different spots of the corresponding dioxide surface, with the aim of both confirming the samples homogeneity and enhancing the signal-to-noise ratio of the final spectra. In general terms, the UO_2 Raman spectrum presents its two well-reported main features at ~445 cm^{-1} (T_{2g} mode) and ~1150 cm^{-1} (2LO phonon overtone).[23,24] As for the Ce-containing samples, a remarkable additional feature is observed around 500-600 cm^{-1}, which continuously increases in intensity with increasing Ce content. Indeed, this feature grows in such a way that it even exceeds the intensity of the other bands at high doping concentrations. The Raman spectrum of pure CeO_2, on the other hand, shows the expected single T_{2g} mode at 465 cm^{-1}.[25]

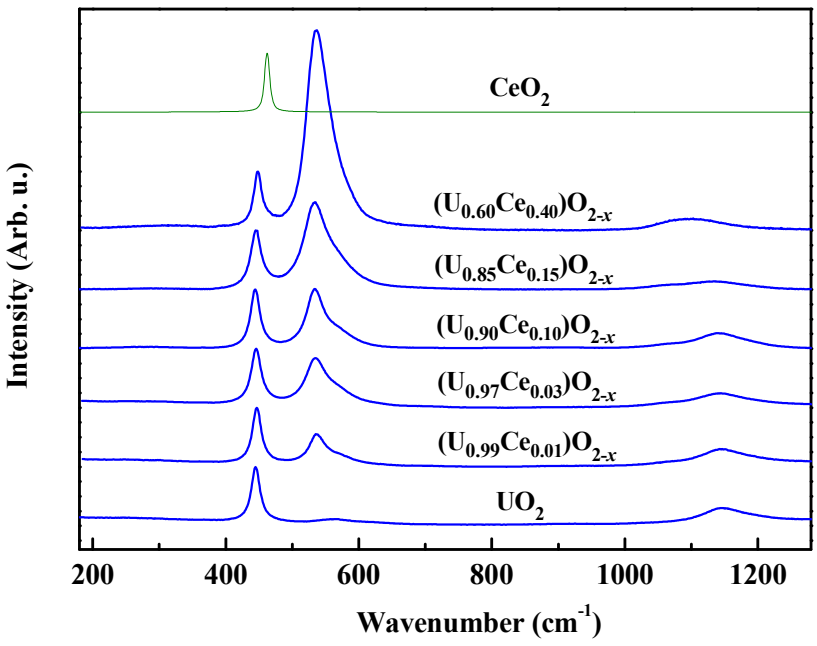

Fig. 2. Raman spectra of pure UO_2 and CeO_2 and the sintered $(U_{1-y}Ce_y)O_{2-x}$ oxides, with $0.01 \leq y \leq 0.40$.

In order to better examine the spectra evolution as a function of Ce incorporation within the UO_2 fluorite-like structure, a detailed peak-profile analysis was conducted making use of Lorentzian bandshapes. Figure 3 shows the UO_2 and $(U, Ce)O_{2-x}$ Raman spectra with the different contributions extracted from their corresponding profile fitting. The resulting fitted profiles are also shown for comparison purposes.

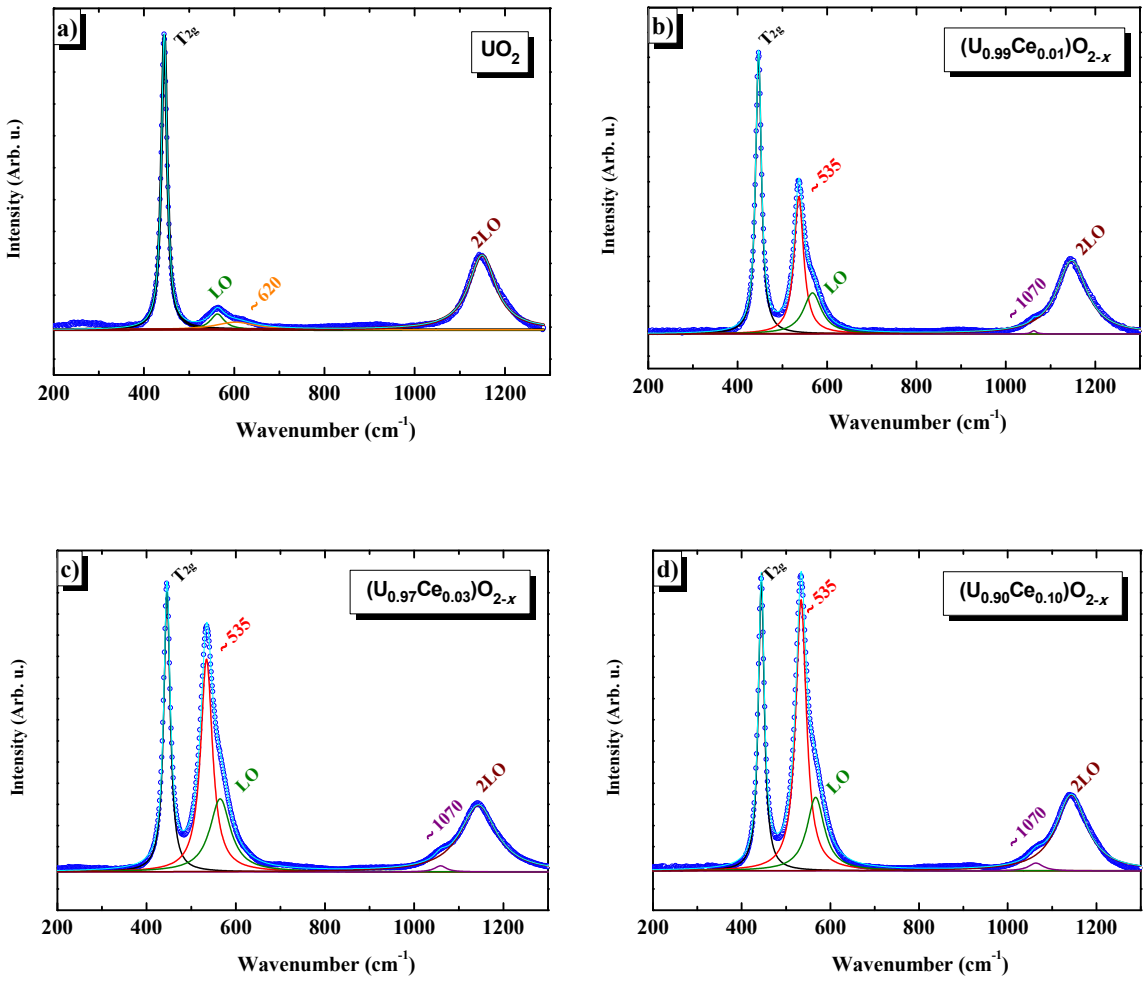

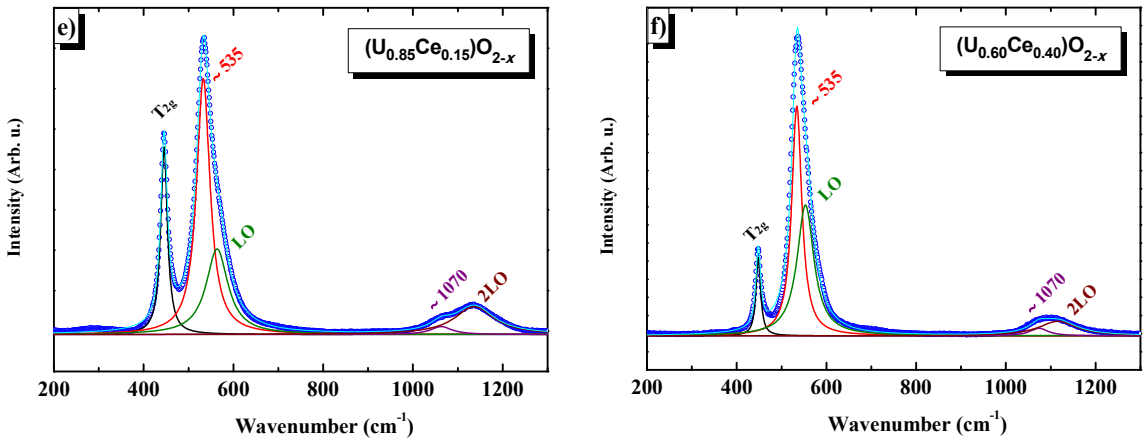

Fig. 3. Profile analysis of the different $(U_{1-y}Ce_y)O_{2-x}$ Raman spectra ($0 \leq y \leq 0.4$).

In the case of pure UO_2, apart from the T_{2g} and 2LO characteristic bands, two weak bands are observed at ~575 cm^{-1} and ~620 cm^{-1} (see Figure 3a), which are usually associated with lattice defects.[26-29] In particular, some studies have assigned a band at ~575 cm^{-1} to the LO mode and its observation has been related to a breakdown in the selection rules due to lattice distortions.[27,28] Likewise, a band around 620-630 cm^{-1} has often been attributed to oxidation, more precisely to cuboctahedral clusters formation due to further oxidation to U_4O_9.[27-30] The appearance of the latter features in the UO_2 spectrum might thus indicate that a minor surface oxidation affects slightly the lattice ordering. In accordance with the experimental equations published elsewhere,[29] the oxidation degree of such hyperstoichiometric UO_{2+x} would roughly correspond to $x \sim 0.07$.

Raman spectra shown in Figures 3b-3f correspond to Ce-containing samples and present five bands. In addition to T_{2g}, LO and 2LO peaks, two features are observed around 535 cm^{-1} and 1070 cm^{-1}; but in this case the ~620 cm^{-1} band is not observed, thus indicating that not even surface oxidation has been produced.

A single-peak contribution is noticed for the T_{2g} band of all the mixed oxides, what ascertains that it follows a one-mode vibration model, as expected for heavy metal dioxides mixtures.[31,32] The variation of this band position with Ce content has been quantitatively analysed in Figure 4 and compared to the expected values (dotted line in Figure 4), which have been calculated taking into

account the influence on the T_{2g} Raman shift of the changes produced in both the reduced mass and force constant by Ce incorporation. The force constant dependency on the interatomic distance has been modelled using the Guggenheimer model as described by Jules and Lombardi.[33] As can be seen, a small upshift is detected, just ~3 cm^{-1} up to $(U_{0.60}Ce_{0.40})O_{2-x}$ instead of the slightly larger move that should be observed if assuming a one-mode behaviour, where the T_{2g} band would upshift on a proportional basis as Ce concentration increases, from pure UO_2 to CeO_2 corresponding wavenumbers.[34] For instance, this is what occurs in the case of $(U,Pu)O_2$: the T_{2g} band, which presents one-mode vibration behaviour,[35-38] shifts towards higher wavenumbers between its position in UO_2 and that in PuO_2 as a function of Pu content.[37,38] The observed small upshift for $(U,Ce)O_2$ oxides was already noticed by Ravindran and Krishnan,[15] who reported it to be "only of the order of 5 cm^{-1} over 80 at.% substitution of cerium". These authors did not provide any explanation, but claimed that the contrast observed with regard to $(U, Pu)O_2$ indicates a quite different effect of Pu and Ce on UO_2. We suggest that the contribution of Ce^{4+}-O bonds, which are shorter[19] and hence stiffer than U-O bonds in the fluorite-like structure, is partially balanced with the weakness produced by the presence of stable oxygen vacancies in the surroundings of Ce^{3+} atoms, as also deduced from the X-ray diffraction analysis.

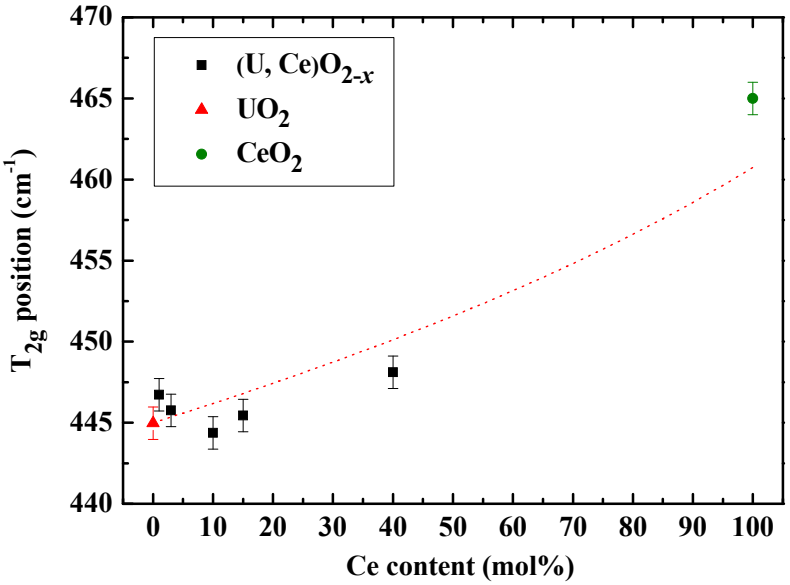

Fig. 4. T_{2g} band position of the characterised $(U_{1-y}Ce_y)O_{2-x}$ oxides as a function of Ce content ($0.01 \leq y \leq 0.4$). The corresponding values obtained for pure UO_2 and CeO_2 are also included. The dotted line represents the expected values according to changes in both force constants (interatomic distance) and reduced mass.

Furthermore, since various studies have associated a peak observed around 530-540 cm^{-1} with the presence of oxygen vacancies,[10-14,28] the occurrence of a band at ~535 cm^{-1} in the mixed oxides spectra (Figures 3b-3f) would confirm the reported presence of Ce^{3+} ions that lead to creation of stable oxygen vacancies.[1] On the other hand, to the best of our knowledge, no mention to the band found at ~1070 cm^{-1} has been made in the literature before. Indeed, these two new bands in the spectra of Ce-containing samples seem to continuously grow with the increase in Ce content, especially the one at ~535 cm^{-1}, which corroborates the increasing presence of Ce^{3+} atoms that lead to a growing amount of oxygen vacancies. Such evolution has been quantitatively estimated by analysing, as a function of Ce content, the area ratio of both bands with respect to that of the T_{2g} band (A_{535}/A_{T2g} and A_{1070}/A_{T2g}). As can be seen in Figure 5, the two bands experiment a linear growth with the increase in Ce content.

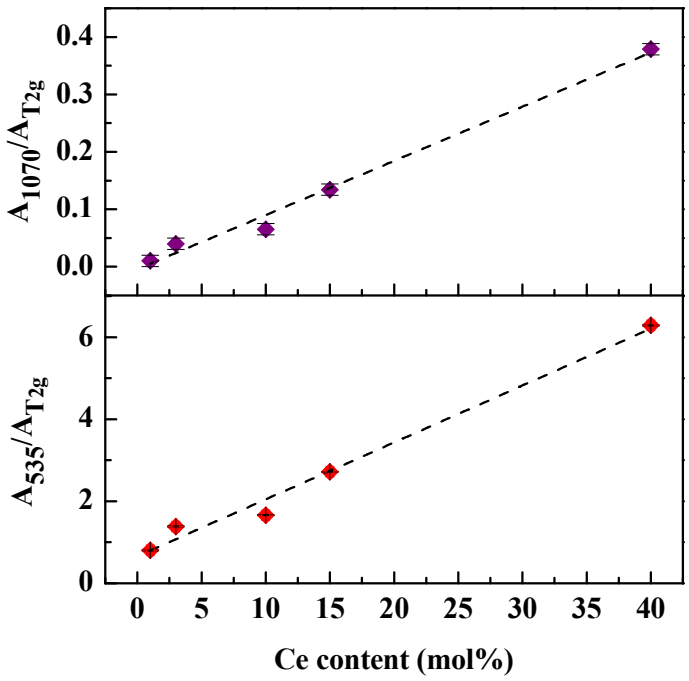

Fig. 5. Evolution with Ce content of the normalised area, with respect to the T_{2g} band, of the ~535 cm^{-1} and ~1070 cm^{-1} bands.

This parallel behaviour, as well as the fact that the wavenumber value of the ~1070 cm^{-1} band is precisely twice the one corresponding to the ~535 cm^{-1} band, suggest that the ~1070 cm^{-1} band is actually the first overtone of the latter band. Moreover, the following additional information can be

inferred from the observed proportional relation between these two bands: none of them corresponds to a resonance Raman band and both are symmetry-allowed in the same manner, in contrast to the case of the LO band and its 2LO overtone in the Raman spectrum of UO_2.[27]

Post-oxidation characterisation

After the air oxidation treatment, which consisted in the 10°C/min heating ramp and the subsequent three hours isotherm at 350ºC, a detailed Raman spectroscopy analysis was performed on all the oxidised $(U_{1-y}Ce_y)O_{2-x}$ specimens ($0 \leq y \leq 0.40$) in order to examine the influence of Ce content in the dioxide oxidation.

Except for pure UO_2, where complete oxidation to U_3O_8 was detected in various zones of the sample surface as shown in Figure 6, the intermediate M_4O_9 phase (M=U,Ce) was found to stabilise in all cases.[30] This is reflected in Figure 7, which gathers the spectra acquired for the different uranium-cerium mixed oxides, as well as for UO_2 on the zones that had not been completely turned into U_3O_8 (light areas in Figure 6a). Again, each Raman spectrum consists of the sum of ~10 similar spectra obtained on distinct spots of the corresponding dioxide surface. The various contributions extracted from the peak-profile analysis of these Raman spectra over the 350-750 cm^{-1} range are included.

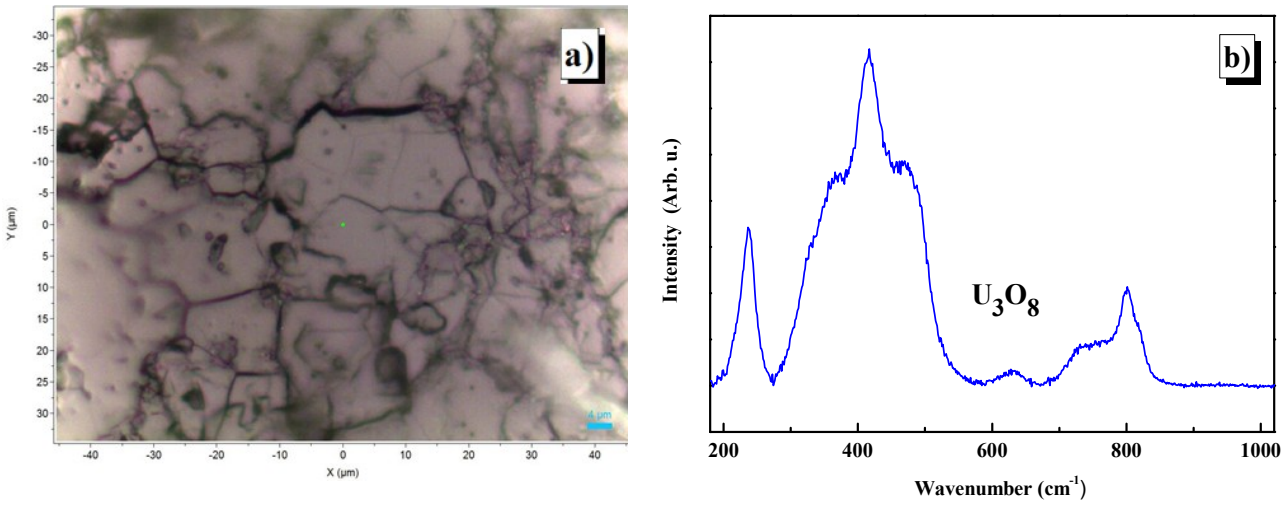

Fig. 6. a) Optical image of the oxidised UO_2 sample surface. b) Typical Raman spectrum of U_3O_8,[39,40] acquired on the dark shiny areas in a).

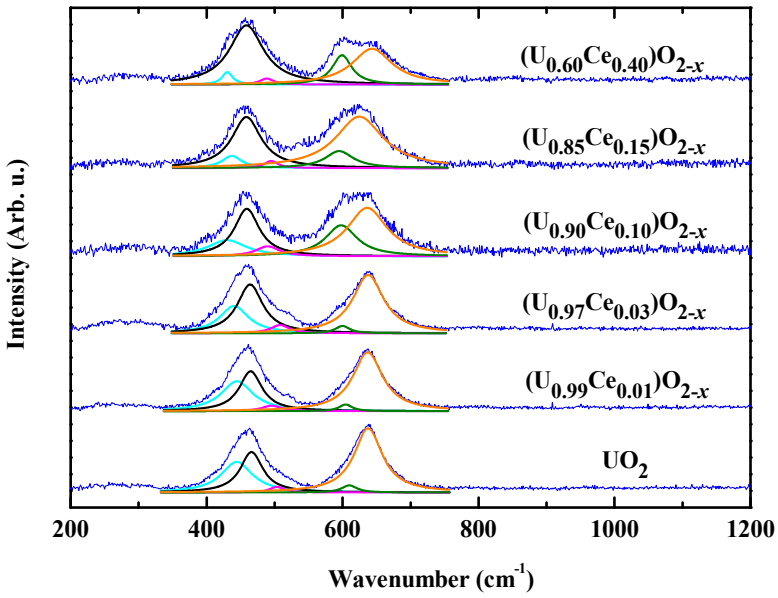

Fig. 7. Raman spectra corresponding to the oxidised $(U_{1-y}Ce_y)O_{2-x}$ samples ($0 \leq y \leq 0.4$). Lorentzian peaks obtained from their profile analysis are also plotted.

In this way, each oxide features the same five bands over the studied range. The three peaks observed at ~435, ~460 and ~495 cm^{-1} might correspond to the splitting of the triply degenerate T_{2g} band due to symmetry loss, as occurs when it is transformed to the orthorhombic U_3O_8 phase.[39,40] The other peaks located at ~605 and ~635 cm^{-1} seem to be the LO and oxidation-related bands, accordingly, although now considerably shifted with respect to their pre-oxidation positions. Indeed, Desgranges *et al.* observed in U_4O_9 a similar broad band centred on ~630 cm^{-1} which they associated with oxidation.[30]

Therefore, an oxidation degree comparison of the treated $(U, Ce)O_{2-x}$ oxides was carried out by analysing the area ratio of the ~635 cm^{-1} band with respect to that of the T_{2g} band (A_{635}/A_{T2g}) in each case. The ~460 cm^{-1} peak was taken as a reference of T_{2g} for the analysis, since it is the most representative among the triplet if considering a single broad T_{2g} band. As can be seen in Figure 8a, the latter area ratio decreases in general terms as a function of Ce content, suggesting the detection of higher oxidation degrees on U-richer samples. For greater reliability, the T_{2g} band shift undergone by every oxide, with regard to its corresponding pre-oxidation position, was also

examined. This method allows us to extract the oxidation contribution, as previously performed on heat treated (U, Pu)O_2 oxides.[38] Figure 8b shows how the studied shift is continuously smaller, and thus the oxidation degree lower, as Ce concentration increases, in good agreement with the results obtained from the preceding analysis.

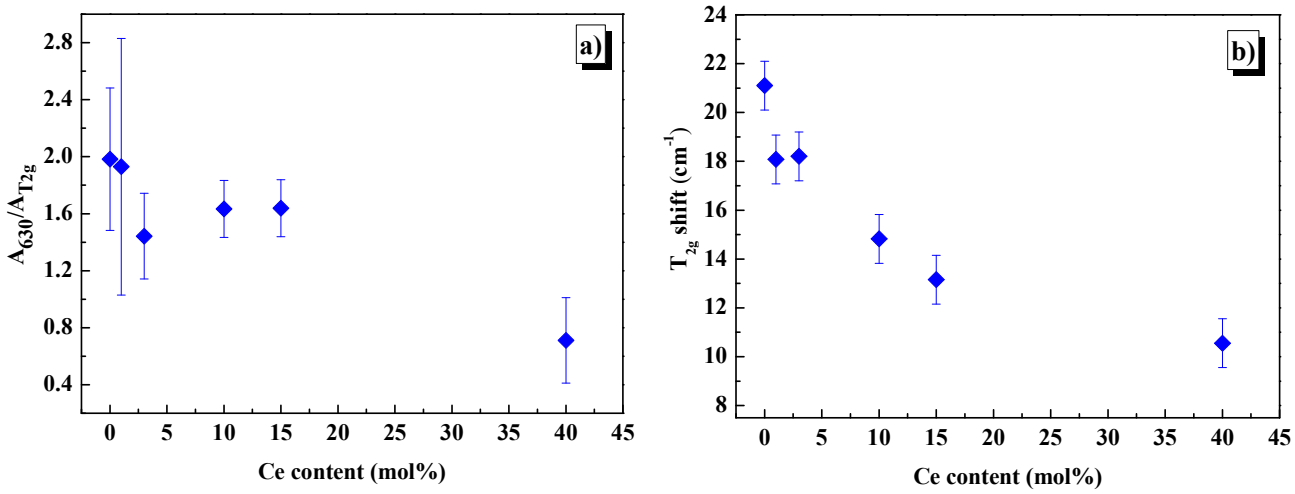

Fig. 8. a) Evolution of the normalised area –with respect to T_{2g} band– of the ~630 cm^{-1} oxidation-related peak and b) T_{2g} band shift due to oxidation, as a function of Ce content.

The latter tendency, observed by the sole means of Raman spectroscopy in this work, is in line with the previously noticed hindering effect on (U, Ce)O_2 oxidation caused by the increasing presence of Ce,[2,5] what might be attributed to a diminished oxygen mobility in the contracted lattice. In addition, unlike UO_2, Ce-containing dioxides presented no trace of further oxidation to M_3O_8; not even the one with only 1 mol% substituted. Thus, these Raman results also confirm that the presence of Ce within the UO_2 lattice helps to preserve the dioxide integrity longer, *i.e.* to resist the formation of M_3O_8.[2,5] A similar effect due to the presence of Pu within the UO_2 fluorite structure has been recently noted,[38] pointing out the comparable overall behaviour of (U, Ce)O_2 and (U, Pu)O_2 against oxidation.

4. CONCLUSIONS

Pre- and post-oxidation Raman characterisation has been conducted on various $(U_{1-y}Ce_y)O_{2-x}$ oxides, with y = 0.01, 0.03, 0.10, 0.15, 0.40, in order to attain a better understanding of the structural features of these uranium-cerium mixed dioxides.

In this way, previous to oxidation, the evolution of UO_2 Raman spectrum as a function of Ce incorporation has been examined. The linear increase with Ce content of the band related to vacancies, located at ~535 cm^{-1}, confirms the previously reported presence of Ce^{3+} ions. Besides, a new band found at ~1070 cm^{-1} has been proposed as the first overtone of the latter band, since it follows the same growing behaviour with Ce content. The T_{2g} band position has also been studied as a function of Ce concentration, showing a smaller upshift than that expected; a fact that can be interpreted as an evidence of the vacancies influence in the corresponding cations surroundings.

With regard to the oxidised samples analysis, it has been observed that the oxidation degree attained is less significant as Ce concentration increases, what sustains the protective effect of Ce. Furthermore, comparison with pure UO_2 indicates that even 1 mol% Ce doping is sufficient to induce a hindering effect on the dioxide matrix oxidation, resisting M_3O_8 formation and stabilising the M_4O_9 phase on the time scale studied.

Thus, it can be concluded that (U, Ce)O_2 behaves, in general terms, like (U, Pu)O_2, at least with regard to the delay it provokes on the dioxide matrix oxidation. Nevertheless, care should be taken when comparing them at a local level, since our Raman spectroscopy analysis reveals that the structure of these two materials is not exactly similar. This raises the question as to whether it is certainly adequate to use (U, Ce)O_2 as a surrogate for MOX fuel in research studies.

ACKNOWLEDGEMENTS

This work was supported by ENRESA within the project Nº 079000189, entitled "Aplicación de técnicas de caracterización en el estudio de la estabilidad del combustible nuclear irradiado en condiciones de almacenamiento" (ACESCO). VGB acknowledges support from MINECO under project CTQ2015-67755-C02-01-R.

DATA AVAILABILITY

The raw/processed data required to reproduce these findings cannot be shared at this time as the data also forms part of an ongoing study.

REFERENCES

[1] S. Bera, V. K. Mittal, R. V. Krishnan, T. Saravanan, S. Velmurugan, K. Nagarajan and S. V. Narasimhan, *J. Nucl. Mater.*, **393**, 120-125 (2009).

[2] H. P. Nawada, P. Sriramamurti, K. V. Govindan Kutty, S. Rajagopalan, R. B. Yadav, P. R. Rasudeva Rao and C. K. Mathews, *J. Nucl. Mater.*, **139**, 19-26 (1986).

[3] P. Martin, M. Ripert, T. Petit, T. Reich, C. Hennig, F. D'Acapito, J. L. Hazemann and O. Proux, *J. Nucl. Mater.*, **312**, 103-110 (2003).

[4] K. S. Kumar, T. Mathews, H. P. Nawada and N. P. Bhat, *J. Nucl. Mater.*, **324**, 177-182 (2004).

[5] T. L. Markin, R. S. Street and E. C. Crouch, *J. Inorg. Nucl. Chem.*, **32**, 59-75 (1970).

[6] Y. Hinatsu and J. Fujino, *Chem. Phys. Lett.*, **172**, 131-136 (1990).

[7] T. R. Griffiths, St. HV, A. Hubbard and M. J. Davies, *Inorg. Chim. Acta*, **225**, 305-317 (1994).

[8] S. -H. Kang, J. -D. Yi, H. -I. Yoo, S. -H. Kim and Y. W. Lee, *J. Phys. Chem. Solids*, **63**, 773-780 (2002).

[9] B. E. Hanken, C. R. Stanek, N. G-Jensen and M. Asta, *Phys. Rev. B*, **84**, 085131-1-085131-9 (2011).

[10] J. R. McBride, K. C. Hass, B. D. Poindexter and W. H. Weber, *J. Appl. Phys.*, **76**, 2435 (1994).

[11] L. Desgranges, Y. Pontillon, P. Matheron, M. Marcet, P. Simon, G. Guimbretière and F. Porcher, *Inorg. Chem.*, **51**, 9147-9149 (2012).

[12] Z. Talip, T. Wiss, P. E. Raison, J. Paillier, D. Manara, J. Somers and R. J. M. Konings, *J. Am. Ceram. Soc.*, **98**, 2278-2285 (2015).

[13] J. Lee, J. Kim, Y. -S. Youn, N. Liu, J. -G. Kim, Y. -K. Ha, D. W. Shoesmith and J. -Y. Kim, *J. Nucl. Mater.*, **486**, 216-221 (2017).

[14] M. Razdan and D. W. Shoesmith, *J. Electrochem. Soc.*, **161**, H105-H113 (2013).

[15] T. R. Ravindran and R. V. Krishnan, *Vib. Spectrosc.*, **73**, 97-101 (2014).

[16] J. Auborn and J. Choo, *Adv. Powder Metall. Part. Mater.*, **2**, 17-25 (1993).

[17] S. Fernández, M. I. Nieto, J. Cobos and R. Moreno, *J. Eur. Ceram. Soc.*, **36**, 3505-3512 (2016).

[18] Certificate of Analysis, Standard Reference Material 674b, X-ray Powder Diffraction Intensity Set for Quantitative Analysis by X- ray Powder Diffraction, National Institute of Standards and Technology (2005).

[19] R. V. Krishnan, G. Panneerselvam, B. M. Singh, B. Kothandaram, G. Jogeswararao, M. P. Anthony and K. Nagarajan, *J. Nucl. Mater.*, **414**, 393-398 (2011).

[20] D. J. Kim, Y. S. Kim, S. H. Kim, J. H. Kim, J. H. Yang, Y. W. Lee and H. S. Kim, *Thermochim. Acta*, **441**, 127-131 (2006).

[21] R. D. Shannon, *Acta Cryst.*, A**32**, 751-767 (1976).

[22] R. K. Hailstone, A. G. DiFrancesco, J. G. Leong, T. D. Allston and K. J. Reed, *J. Phys. Chem. C*, **113**, 15155-15159 (2009).

[23] P. G. Marlow, J. P. Russell and J. R. Hardy, *Philos. Mag.*, **14**, 409-410 (1966).

[24] T. Livneh and E. Sterer, *Phys. Rev. B*, **73**, 085118-085119 (2006).

[25] V. G. Keramidas and W. B. White, *J. Chem. Phys.*, **59**, 1561-1562 (1973).

[26] P. R. Graves, *Appl. Spectrosc.*, **144**, 1665-1667 (1990).

[27] H. He and D. Shoesmith, *Phys. Chem. Chem. Phys.*, **12**, 8108-8117 (2010).

[28] G. Guimbretière, L. Desgranges, A. Canizares, G. Carlot, R. Caraballo, C. Jégou, F. Duval, N. Raimboux, M. R. Ammar and P. Simon, *Appl. Phys. Lett.*, **100**, 251914 (2012).

[29] J. M. Elorrieta, L. J. Bonales, N. Rodriguez-Villagra, V. G. Baonza and J. Cobos, *Phys. Chem. Chem. Phys.*, **18**, 28209-28216 (2016).

[30] L. Desgranges, G. Baldinozzi, P. Simon, G. Guimbretière and A. Canizares, *J. Raman Spectrosc.*, **43**, 455-458 (2012).

[31] I. Chang and S. Mitra, *Phys. Rev.*, **172**, 924 (1968).

[32] D. Peterson, A. Petrou, W. Giriat, A. Ramdas and S. Rodriguez, *Phys. Rev. B*, **33**, 1160 (1986).

[33] J. L. Jules and J. R. Lombardi, *J. Mol. Struct. (Theochem)*, **664-665**, 255–271 (2003).

[34] L. Genzel, T. P. Martin and C. H. Perry, *Phys. Stat. Sol.(b)*, **62**, 83-92 (1974).

[35] Z. Talip, S. Peuget, M. Magnin, L. Berardo, C. Valot, R. Vauchy and C. Jégou, *J. Raman Spectrosc.*, **48 (5)**, 765-772 (2017).

[36] C. Jégou, R. Caraballo, S. Peuget, D. Roudil, L. Desgranges and M. Magnin, *J. Nucl. Mater.*, **405**, 235-243 (2010).

[37] R. Böhler, M. J. Welland, D. Prieur, P. Cakir, T. Vitova, T. Pruessmann, I. Pidchenko, C. Hennig, C. Guéneau, R. J. M. Konings and D. Manara, *J. Nucl. Mater.*, **448**, 330-339 (2014).

[38] J. M. Elorrieta, D. Manara, L. J. Bonales, J. F. Vigier, O. Dieste, M. Naji, R. C. Belin, V. G. Baonza, R. J. M. Konings and J. Cobos, *J. Nucl. Mater.*, **495**, 484-491(2017).

[39] G. C. Allen, I. S. Butler and N. A. Tuan, *J. Nucl. Mater.*, **144**, 17-19 (1987).

[40] I. S. Butler, G. C. Allen and N. A. Tuan, *Appl. Spectrosc.*, **42 (5)**, 901-902 (1988).